Correlations in semiconductor ring laser in the bidirectional regime

Antonio Pérez S.

July 19, 2007

Agradecimientos

Quiero agredecer al director de esta memoria, Alessandro Scirè, su confianza y empeño para que en un futuro me convierta en un científico. También quiero agradecer a Roberta Zambrini su ayuda, sin la cuál esta memoria no hubiese sido posible.

Gracias también a los profesores Maxi San Miguel, Raúl Toral, Pere Colet, Claudio Mirasso y Salvador Balle, por su ayuda directa o indirecta en la elaboración de esta memoria.

También quiero dar las gracias a los compañeros y compañeras del IFISC y del Máster en Física, como también a Rubén Tolosa y Susana Sánchez por su ayuda técnica.

Contents

Chapter 1

Introduction

As a source of coherent radiation, the Laser found numerous applications since it appeared in the early 1960s, starting from welding sheets in the vehicle construction industry in 1969, ranging today from optical communications, to medicine, military and leisure use.

Optical communications had a enormous growth in the last decades thanks to the development of optical fibers and the capacity to modulate lasers at high frequencies. In this field lasers are used as sources of digital messages and to characterize optical fibers.

In metrology, lasers are used to make accurate geodesic measurements e.g. to measure the earth bark and rotation movements. They are used to measure the pollution in the atmosphere and to measure the Moon-Earth distance. They were used in relativity experiments and to measure the speed of light with a great precision and in spectroscopy. Lasers are used in materials and molecular structure characterization and can induce chemical reactions in selective form.

As industrial applications, lasers are used to weld, melt or vaporize materials with high precision in many different fields, from jewellery to aeronautics. Lasers are used to cut microelectronics components, to warm up semiconductors chips, to cut textile patterns o synthesize materials. In the construction of roads and buildings they are used to align structures and measure distances. Another important field for laser is medicine, surgery in particular.

The guiding laser systems for missiles, aircrafts and satellites are one of the numerous military applications of lasers. Also they are use in the navi-

gation systems of planes and ships.

For our leisure time we can find laser applications in music in our compact-disk (CD) player or staring light shows in live show. After CD, CD-ROM and DVD allow to store and manage a great amount of data.

A laser is constructed from three principal parts:

- An energy source (usually referred to as the **pump** or **pump source**),

- A **gain medium** or laser medium, and

- A cavity that forms an **optical resonator**.

The type of pump source used in practice depends on the choice of active medium, and this also determines how the energy is transmitted to the medium. Examples of pump sources include electrical discharges, flashlamps, arc lamps, light from another laser, chemical reactions and even explosive devices. A He-Ne laser uses an electrical discharge in the helium-neon gas mixture, a Nd:YAG laser uses a light focused from a xenon flash lamp, and semiconductor laser uses a simple electric current.

The gain medium severely affects the operation wavelength of the laser. The gain medium is excited by the pump source to produce a population inversion, providing optical gain and thus amplification.

Usually the cavity is formed by two parallel mirrors placed around the gain medium which provides optical feedback. This is the Fabry-Perot optical cavity. Another possible optical resonator is the ring cavity. In the ring cavity two laser beams propagate in opposite directions. Historically ring lasers were made by tubes of He-Ne and corner mirrors, but recently lithography technology enabled the fabrication of semiconductor ring laser in various different shapes.

1.1 Ring laser

A peculiar application of the ring laser is the gyroscope, an instrument to measure inertial rotations. The operation principle is the following, in the ring cavity two optical modes propagate in opposite directions, a measure of the interference pattern formed by extracting and heterodyning portions of the two counter propagating beams provides information about the rotation

rate relative to an inertial frame.

The idea of using a ring interferometer as a rotation rate sensor was introduced by Sagnac in 1913 but, until the demonstration of the laser, the Sagnac interferometer was not considered as an alternative to conventional mechanical gyroscopes. The advantage of the ring laser gyroscope as a rotation sensing device is that it has no moving parts and so would seem, potentially, to have a longer repair lifetime than a mechanical gyroscope, but the major advantage is the higher sensitivity (the minimum rotation that the instrument can resolve) attaining $(0.001°/h)$.

There are two major types of laser gyroscopes: the ring laser gyroscopes and the fiber ring gyroscopes. The ring laser gyroscope has higher sensitivity than fiber gyroscope and is used for ultra-high sensitivity measurements [1], e.g. to measure the Earth's rotation. Fiber ring gyroscopes [2] are cheaper and used in commercial applications, like in the navigation systems of aircrafts.
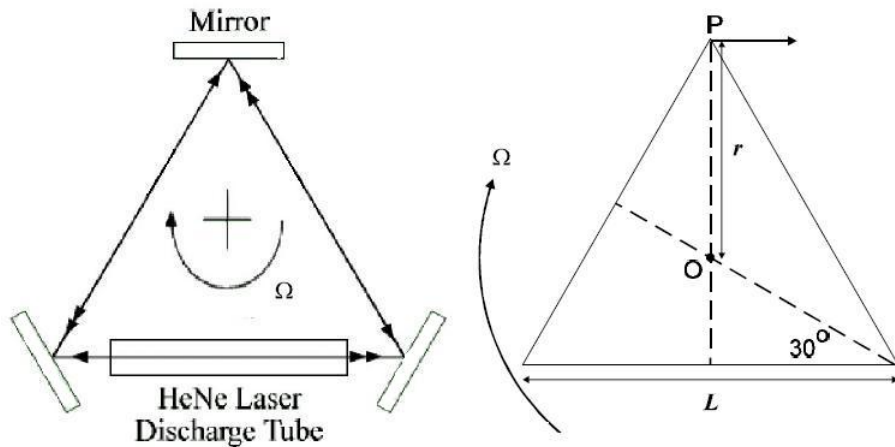

Figure 1.1: Scheme of the He-Ne ring laser gyroscope.

Sagnac effect

The basis for the description of the operation of a ring laser gyroscopes is the called Sagnac effect. By considering the scheme shown in figure 1.1, we suppose that the light leaves the point P of the triangular cavity, rotating around O with an angular velocity Ω. The time it takes in return to P making

the travel in the ring cavity if $\Omega = 0$ is $t = \frac{3L}{c} = \frac{S}{c}$. Where L is the length of the side of the triangle and $S = 3L$ is the total perimeter. When the gyroscope spins (i.e. $\Omega \neq 0$), the point P moves to a distance $d = \Omega r t = \Omega r \frac{S}{c}$, where r is the distance from P to O, which is $\frac{L}{2} \sec 30° = \frac{L}{\sqrt{3}}$. The change of optical path δS seen by the beam is the component of the movement of P along the direction of the beam, which is: $\delta S = d \cos 60° = d/2$, making use of d and r one arrives to:

$$\delta S = \frac{\Omega S L}{2c\sqrt{3}} = \frac{\sqrt{3}\Omega L^2}{2c} \qquad (1.1)$$

And now using the area of a triangle, $A = \frac{\sqrt{3}L^2}{4}$, we got:

$$\delta S = \frac{2\Omega A}{c} \qquad (1.2)$$

To accomplish with the cavity resonance condition, the path length is a integer number of times the wavelength, $m\lambda = 3L = S$, therefore for a change δS a change $\delta \lambda$ is produced:

$$\delta\lambda = \frac{\delta S}{m} = \frac{\lambda \delta S}{S} \qquad (1.3)$$

And the correspondent frequency change is $\delta\nu/\nu = \delta\lambda/\lambda = \delta S/S$. Each beam suffers the same change in frequency, but in opposite direction, therefore the beat frequency f is $f = 2\delta\nu = 2\nu(\delta S/S)$, and using (1.2) one obtains:

$$f = \frac{4\Omega A \nu}{cS} = \frac{4\Omega A}{\lambda S} \qquad (1.4)$$

This is the basic equation to model the measurement of angular rotations. In [3] a derivation of the Sagnac effect in the context of general relativity is reported.

In principle, laser gyroscopes should be very sensitive and accurate with a fundamental limit of less than 10^{-6} °/h. In practice the performance is less than this, the limits being set by the accuracy of fabrication, cleanliness and a few inherent operational difficulties. The use of the device as a rotation sensor depends crucially on the extent to which the relation (1.4) is valid. In the ideal case (that is, one which obeys (1.4)) the relationship between Ω and f is linear as shown in figure 1.2.

There are three main kinds of error that may cause relation (1.4) to be invalid.
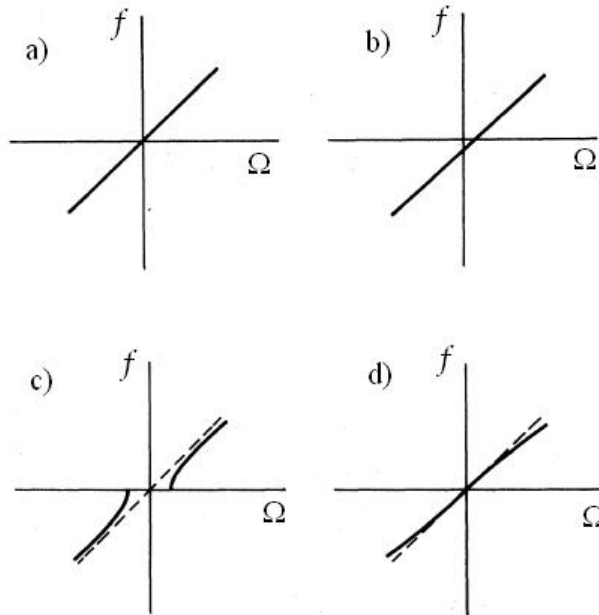
Figure 1.2: Beat frequency f vs input rotation rate Ω in a ring laser gyro. a) The ideal case, a straight line through the origin; b) A linear relationship with a nonzero null shift; c) Frequency locking; and d) nonlinearities in the response (variable scale factor). [3].

1. **Null shift** (fig. 1.2 (b)). This happens when the frequency difference is "biased", i.e. f is non zero for zero input rate. It amounts to adding a constant term to the right-hand side of (1.4), the exact magnitude of which is unpredictable. It can arise from any anisotropy in the cavity respect to the radiation traveling in the two directions. If it is constant and repeatable it can be measured and compensated for in the final output. If it drifts, however, or changes from turn-on to turn-on, it can be a serious problem. The main cavity anisotropy that gives rise to null shift errors is the Langmuir flow in the active gas laser medium. It consists in a flow appearing in the gas as a consequence of the dc power supply, there is a movement of the neutral atoms which is towards the cathode along the center of the discharge tube, and towards the anode along the walls. Since the laser beam is along the tube center, it sees a net motion of the medium. This effect is used to determinate physical properties of the plasma.
   The usual way to avoid this problem is to make the Langmuir flow

7

reciprocal by using two discharge tubes with opposite polarities. In this way the two "biasing" elements cancel each other. The discharge current has to be the same in both tubes to a rather high accuracy if no null shift is to be observed. The problem can be completely avoided if we use a semiconductor or solid state laser.

2. **Mode locking**. In the figure 1.2 (c) we can see a dead-band where, even though the rotation rate is non-zero , the beat frequency is fixed at zero, i.e. the fringe pattern is stationary. This occurs when the rotation rate becomes very small. The effect is due to interaction effects between the two counter-propagating fields, when on reflection, a small amount of energy is scattered from the mirror surface back into the oppositely traveling beam. If this difference becomes too small the counter-propagating beams will lock together in the same way that coupled mechanical oscillators operating at slightly different frequencies lock together. When the two fields have the same frequency the beat frequency is zero.

3. Variations in the scale factor as a function of the rotation rate (fig. 1.2 (d)). This means that the linearity in (1.4) no longer holds. These **nonlinear effects** may arise by dispersive effects in the laser medium (frequency pulling and pushing). Or as a consequence of some of the techniques used to eliminate mode locking.

In the paper of Chow et al. [3] an equation of motion is derived from Lamb's semiclassical laser theory assumunig $E_+ = E_-$ for the phase angle difference ψ:

$$\dot{\psi} = S\Omega + b\sin\psi \qquad (1.5)$$

Where Ω is the rotation rate, S is the scale factor and b is the backscattering coefficient. Note that $\dot{\psi}$ is basically the beat frequency, what we called f. If $S\Omega \gg b$ the phase difference ψ grows essentially as a linear function of time, as it would do in absence of backscattering. But if $S\Omega < b$ stationary solutions to (1.5) exist, with $\dot{\psi} = 0$, given by:

$$\psi_s = \begin{cases} -\arcsin\frac{S\Omega}{b} \\ \pi + \arcsin\frac{S\Omega}{b} \end{cases} \qquad (1.6)$$

Of this two solutions the second one, having $b\cos\psi_s < 0$ is stable, this mean that no matter what the initial condition is, the evolution of ψ will eventually bring it arbitrarily close to the value ψ_s, for which the right-hand side of equation (1.5) vanishes. That is the frequency difference vanishes, in

spite of the fact that the rotation rate Ω is nonzero. This is what is called mode locking in the literature. In [3] a description of techniques used to avoid mode locking is reported, e.g. introducing a constant bias or an alternating bias.

Noise in the ring laser gyroscope

In the framework of Lamb's semiclassical laser theory, the optical medium was treated quantum mechanically, whereas the electric field was considered to be a classical quantity. However the electric field can be treated in a quantum-mechanical way too. From this point of view the electric field is a superposition of an infinite number of independent quantum-mechanical harmonic oscillators described by their creation or destruction operators. This problem was studied in the late 1960s, finding new effects such as the infinite zero-point energy of the field, the vacuum fluctuations and spontaneous emission.

Due to spontaneous emission the laser field has a random phase and, therefore, the phase of the electric field in the cavity is no longer well determinated, and it becomes a stochastic quantity. This is very important in the use of a ring laser as a gyroscope, because one measures the phase or frequency difference between the two counter-propagating fields. Therefore, the quantum noise influences the output. All other noise sources, as, for example, vibrations of the laser mirrors, can be overcome by some clever technique.

Due to spontaneous emission of the laser atoms the phase of the electric field in the cavity is a stochastic variable. The equation of motion for the phase difference (1.5) now becomes:

$$\dot{\psi} = S\Omega + b\sin\psi + F(t) \tag{1.7}$$

where $F(t)$ is fluctuating force which we assume to be gaussian with mean zero,

$$< F(t) >= 0 \tag{1.8}$$

where $< \ldots >$ denotes the ensemble average. Such stochastic equations are called Langevin equations. The noise causes the system variable to fluctuate around a mean value and according to the fluctuation-dissipation theorem, also causes damping. Comparing the correlation time τ_c (i.e., the decay time of the atoms) with the damping time of the electric field $1/\gamma$ one finds:

$\tau_c \ll 1/\gamma$. Therefore, on the time scale of the electric field we can assume for the two time correlation function:

$$< F(t)F(t') >= 2D\delta(t - t')$$
(1.9)

There are basically two approaches to calculate the average of a function $f(\psi)$ depending on a stochastic variable ψ: the Langevin and the Fokker-Planck methods. In the Langevin approach one solves the equation of motion for ψ in terms of integrals of the fluctuating force $F(t)$, substitutes this back into $f(\psi)$ and performs the average using (1.8) and (1.9) together with the property that $F(t)$ is gaussian. This approach is difficult in many cases, because one is unable to solve the Langevin equation, which is, at least in the problems of interest, nonlinear.

In the Fokker-Planck approach one derives a partial differential equation for the conditional probability $P(t, \psi|t_0, \psi_0)$ - the probability to find at time t the value ψ, given that the value at t_0 was ψ_0 - and substitutes this into the familiar expression for an average:

$$< f(\psi) >= \int d\psi \ P(\psi)f(\psi)$$
(1.10)

This method work fines because in most of the cases one is able to solve the Fokker-Planck equation exactly, in terms of infinite (matrix) continued fractions. The Fokker-Planck equation corresponding to the problem (1.7) is:

$$\frac{\partial P}{\partial t} = -\frac{\partial}{\partial \psi}[(S\Omega + b\sin\psi)P] + D\frac{\partial^2 P}{\partial \psi^2}$$
(1.11)

This equation subject to periodic boundary conditions can be solved approximately in various regions of the rotation rate [3] as well as exactly in terms of infinite continued fractions.

1.2 Semiconductor ring laser

The semiconductor ring laser (SRL) demonstration was made by Liao and Wang in 1980 [4], their device consists in a circular resonator and a straight waveguide through which the lasing emission can be coupled out of the circular resonator. After that SRL have received increasing attention owing to their application in photonic integrated circuits and because they were regarded as promising candidates for wavelength filtering, unidirectional travelling wave operation, and multiplexing/demultiplexing applications. The output coupler is still a source of problems. In 1995 Krauss et al. [5] investigated

three different types of output couplers in order to identify the influence of the coupling geometry on the performance of the lasers.

Different cavity geometries have been proposed, such as square [6], triangular [7], racetrack [8], micro-squares [9] and S section [10].

In 2003 Sorel et al. [11] fabricated different kinds of semiconductor ring lasers of GaAs and AlGaAs like the shown in figure 1.3. They used three integrated photodetectors to characterize the behaviour of the device. Photodetectors 1 and 2 (PD1 and PD2) are output waveguide photodiodes measuring the two counter propagating fields independently, and photodetector 3 (PD3) is the in line photodiode which measures the total power in the ring cavity.
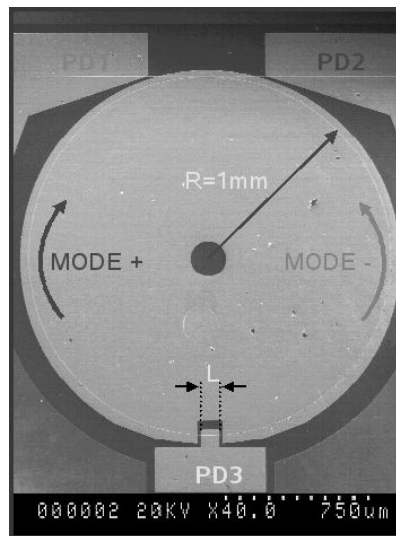

Figure 1.3: Micrograph of the device showing the contact layout with the the ring biasing contact and the three integrated photodetectors. [11]

Experimentally they found different regimes or behaviors for increasing values of the pump coefficient μ described in the figure 1.4. Above threshold the first regime they found is a bidirectional-Continuous Wave regime (labeled Bi-CW), mathematically corresponding to a line of fixed points. After that there is a Hopf bifurcation which marks the beginning of a bidirectional with alternate oscillations regime (Bi-AO), which is a limit cycle in mathematical words. And finally a unidirectional regime (UNI) due to a Pitchfork

11

induced bistability. The latter regime is suitable for applications in optical memories [12].
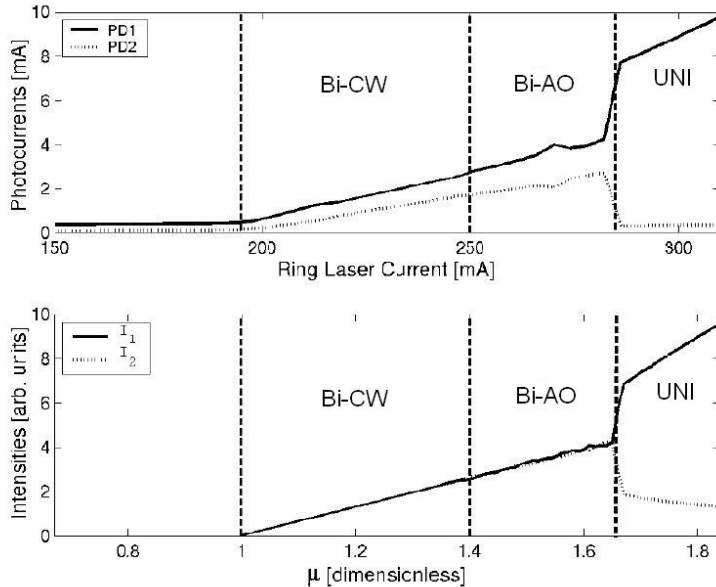

Figure 1.4: Experimental L-I characteristics. The different regimes are indicated. [11]

In this paper [11], the semiconductor ring laser in considered working in a single longitudinal mode, so the electric field inside the cavity is expressed by:

$$E(x,t) = E_+(t)e^{-i(\Omega t - kx)} + E_-(t)e^{-i(\Omega t + kx)} \tag{1.12}$$

Where E_+ and E_- are the mean-field slowly varying complex amplitudes of the electric field associated with the two propagation directions, E_+ clockwise and E_- counter clockwise, respectively. x is the spatial coordinate along the ring, assumed positive in the clockwise direction, and Ω is the optical frequency of the selected longitudinal mode. In [11] the following set of dimensionless rate equations for the time evolution of the electric fields, $E_\pm(t)$, and the carrier density, $N(t)$:

$$\begin{cases} \dot{E}_\pm(t) = \mathcal{G}_\pm(N(t), |E_\pm(t)|^2)\, E_\pm(t) - \eta\, E_\mp(t) \\ \dot{N}(t) = \gamma\, \mathcal{F}(N(t), |E_\pm(t)|^2) \end{cases} \tag{1.13}$$

12

$$\mathcal{G}_{\pm}(N(t), |E_{\pm}(t)|^2) = \frac{1}{2}(1 + i\alpha)\{N(t) \ \sigma_{\pm} - 1\}$$

$$\mathcal{F}(N(t), |E_{\pm}(t)|^2) = \mu - N(t) - N(t) \ \sigma_+ \ |E_+(t)|^2 - N(t) \ \sigma_- \ |E_-(t)|^2$$

$$\sigma_{\pm} = 1 - s \ |E_{\pm}(t)|^2 - c \ |E_{\mp}(t)|^2$$

$$\eta = k_d + ik_c$$

Where η is the complex backscattering coefficient, which is an explicit coupling between the two counter propagating fields, k_d represents the dissipative coupling and k_c the conservative coupling. α takes account of the coupling between phase and amplitudes. The saturations effects in the gain are written in the quadratic approximation, s and c are normalized self- and cross-gain saturation coefficients. μ is the pump parameter and γ is the ratio between the photon lifetime and the carrier lifetime.

Numerical simulations showed that, as the condition $\gamma \ll 1$ is fulfilled, the SRL regimes and dynamics only weakly depend on γ and the carriers adiabatically follow the dynamics of the fields.

They found that it appears that the conservative backscattering acts as a driving force for the alternate oscillations, while dissipative backscattering tends to restore CW operation, either bidirectional or unidirectional depending on the value of the conservative backscattering.

Sorel et al. showed in figure 1.5 the dependence of the frequency of the alternate oscillations versus ring laser pump current. With this data they fitted the parameters of their model finding the following values: $k_d = 0.46 \ 10^{-3}$, $k_c = 8.5 \ 10^{-3}$, $c = 2s = 9.3 \ 10^{-3}$.

The model reported in (1.13) does not take into accounts the influence of spontaneous emission. A commonly accepted form to introduce spontaneous emission is by means of Langevin forces, like we see in the previous section, specifying the problem for a semiconductor lasers. Indeed, in this case there is a coupling between amplitude and phase (α factor) and, due to that we can not derive a Fokker-Planck equation like equation (1.11), therefore we use the Langevin approach solving the nonlinear equations numerically. There are many examples in the literature concerning the noise in semiconductor lasers, see [15] and [16] for example.
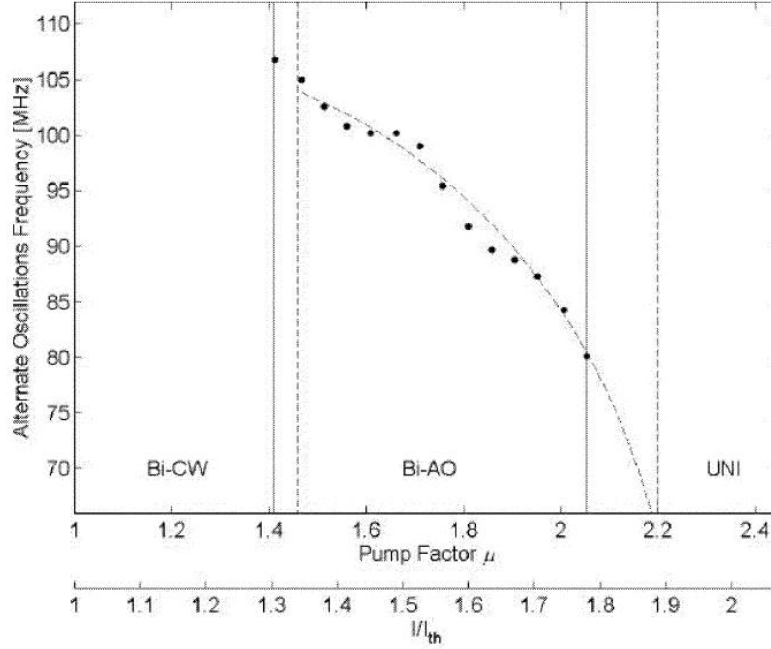
Figure 1.5: Alternate oscillations frequency versus pump current μ. The dots are the experimental data and the dashed curve is the numerical solution of the theoretical model (1.13). [11]

A peculiar noise spectra SRL was found experimentally by Ballantyne and co-workers recently. In [13] they showed the presence in the output spectrum of an unusual low frequency noise peak, that is strongly dependent on the mirror backscattering strength. The mirrors described in the work by Ballantyne et al. were fabricated to embed the medium in a *triangular* ring laser, but also they expected the effect in other geometries like circular or square rings. Moreover noise can induce spontaneous switching in the unidirectional regime (UNI).

The values for the parameters in the text if no others are explicitly indicated are taken from [14] and are: $\alpha = 3.5$, $s = 0.005$, $c = 0.01$, $k_d = 327 \; 10^{-6}$, $k_c = 44 \; 10^{-4}$, $\gamma = 2 \; 10^{-3}$ and $\mu = 1.2$ which corresponds to the bidirectional continuous wave regime (Bi-CW).

Chapter 2

Theoretical analysis

By introducing a fluctuation term (Langevin forces) in the differential equations (1.13) makes them loose its deterministic characteristic and become stochastic differential equations [15]. The numerical method to solve the equations is described in Appendix A. The inclusion of a complex fluctiation term in the equations for the electric fields (1.13) leads to the following stochastic rate equations,

$$\begin{cases} \dot{E}_\pm(t) = \mathcal{G}_\pm(N(t), |E_\pm(t)|^2) \ E_\pm(t) - \eta \ E_\mp(t) + \xi_\pm(t) \\ \dot{N}(t) = \gamma \ \mathcal{F}(N(t), |E_\pm(t)|^2) \end{cases} . \qquad (2.1)$$
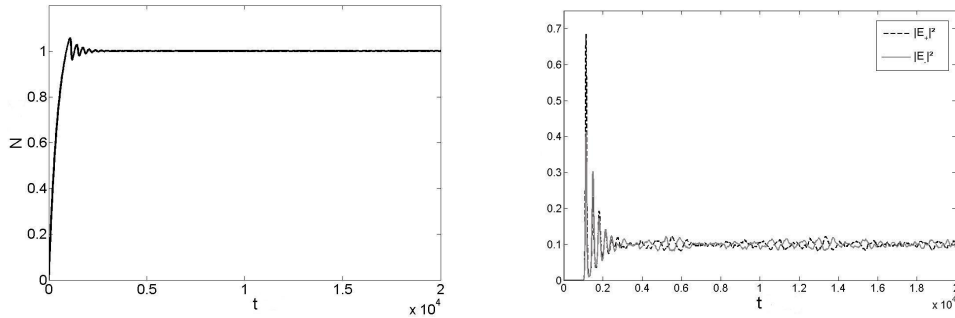

Figure 2.1: Time evolution of the carrier density and the intensities of the fields.

Where $\xi_\pm(t)$ is a white gaussian complex noise with the following correlation properties

$$\begin{aligned} \langle \xi_\pm(t)\xi_\pm^*(t') \rangle &= 2D\delta(t-t') \\ \langle \xi_\pm(t)\xi_\mp^*(t') \rangle = \langle \xi_\pm(t)\xi_\pm(t') \rangle &= \langle \xi_\pm(t)\xi_\mp(t') \rangle = 0. \end{aligned} \qquad (2.2)$$

15

The time traces for the carrier density $N(t)$ and the intensity of the fields $|E_\pm(t)|^2$ are shown in figure 2.1. The system reaches the Bi-CW stationary state after a transient.

2.1 Switch-on statistics

One consequence of the presence of noise is a change in the switch-on time t^*, which results to be statistically distributed. To analyze this one can derive histograms for t^* corresponding to different values of the noise amplitude D, as shown in figures 2.2, 2.3 y 2.4. The total intensity $I(t) = |E_+|^2 + |E_-|^2$ versus dimensionless time is also plotted,
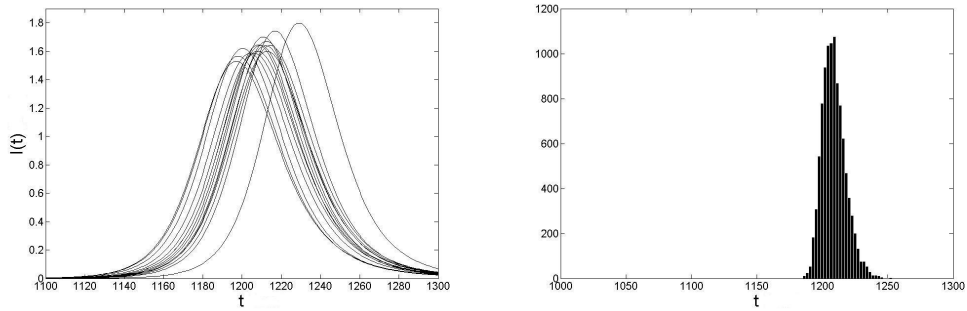

Figure 2.2: Superposition of 15 switch-on and histogram of 10000 realizations, $D = 10^{-4}$.
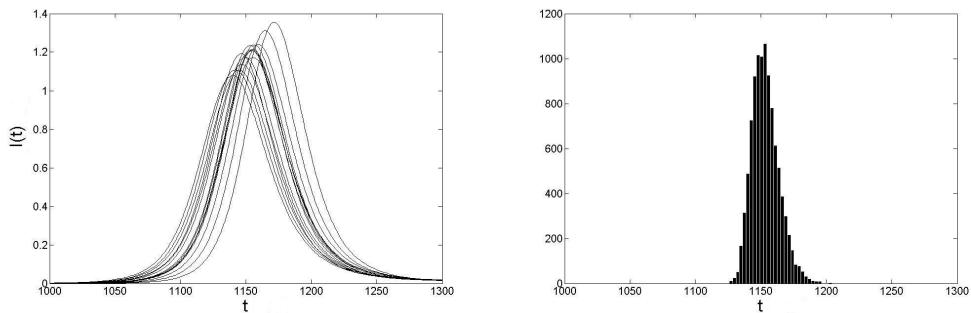

Figure 2.3: Superposition of 15 switch-on and histogram of 10000 realizations, $D = 10^{-3}$.
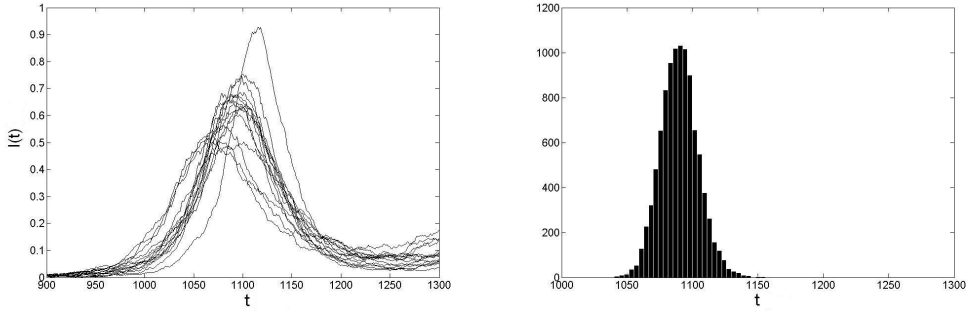
Figure 2.4: Superposition of 15 switch-on and histogram of 10000 realizations, $D = 10^{-2}$.

Figures 2.2, 2.3 and 2.4, show that the distribution of t^* moves toward lower times broadening the distribution. To analyze this behavior more in detail we simulated eqs. (2.1) for values of D ranging from 10^{-4} to 10^{-1}, and deriving a statistics over 10000 realizations. the results are shown in figures 2.5 and 2.6, where the mean value $< t^* >$ of the switch-on time is plotted, as well as its standard deviation, $\sigma_{<t^*>} = \sqrt{(< (t^*)^2 > - < t^* >^2)}$, versus the noise amplitude.
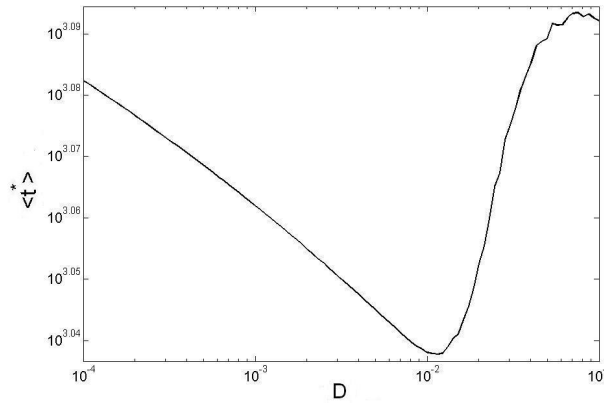

Figure 2.5: Switch-on time mean value $< t^* >$, versus noise amplitude D, both in logarithmic scale.

Figure 2.5 shows that for low noise the mean value of the switch-on time decreases with D, and the deviation increases (fig. 2.6), whereas noise dominates for $D \sim 10^{-2}$.
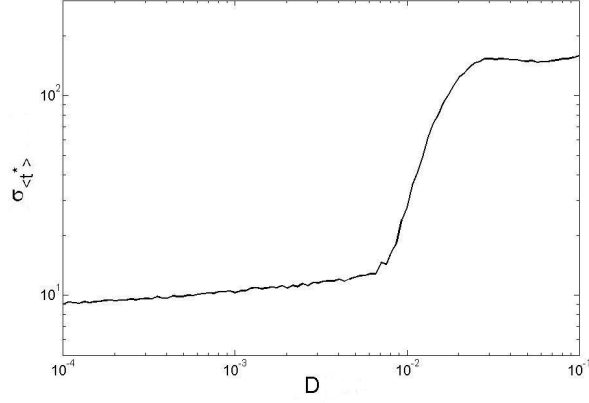
17

Figure 2.6: Switch-on time deviation $\sigma_{<t^*>}$, versus noise amplitude D, both in logarithmic scale.

2.2   Time correlations

In this section the correlations between the two counter propagating fields are analyzed. Correlations are calculated after a transient time of 10^5 time units. In the figures 2.7 and 2.8 the time traces of the electric fields are shown, the figures show that the two-fields intensity dynamics is anticorrelated.
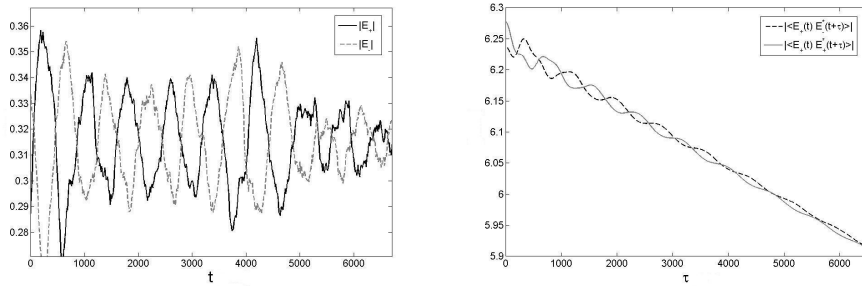

Figure 2.7: Modules of the electric fields after the transient versus dimensionless time, and two times autocorrelation and cross correlation, $D = 10^{-3}$, 20 realizations.
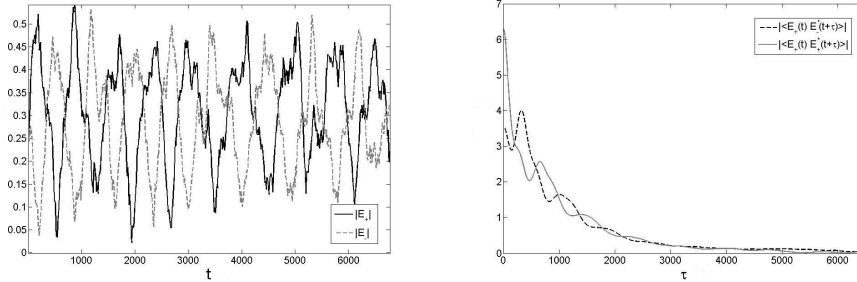
Figure 2.8: Modules of the electric fields after the transient versus dimensionless time,and two times autocorrelation and cross correlation, $D = 10^{-2}$, 20 realizations.

When the noise amplitude D is less or equal to 10^{-3} the two counter propagating fields are strongly correlated (fig. 2.7). Time traces (figs. 2.7 and 2.8) show anticorrelated dynamics for the two fields, as a consequence the cross correlation $< E_+(t)E_-^*(t+\tau) >$, is higher for a non-zero delay τ, whereas the autocorrelation $< E_+(t)E_+^*(t+\tau) >$ is maximum at zero delay. It is so because of a phenomenon called 'noisy precursor' [17]. The system feels the presence of a nearby Hopf bifurcation, noise excites a unstable limit cycle which makes the intensity of the two fields oscillate in anticorrelated fashion. When D increases the correlations tails assume a exponential behavior, as shown in figure 2.8. When noise dominates the dynamical evolution the correlations shrink approaching the Dirac delta function.

2.3 Stationary monochromatic solutions

By substituting the following monochromatic solution for the two fields

$$E_\pm(t) = Q e^{i\omega t \pm i\phi}, \tag{2.3}$$

we find the stationary solutions of (2.1). There are two possible cases,
In phase case:

$$\phi = 0 \rightarrow \omega_{in} = \alpha k_d - k_c \tag{2.4}$$

Out of phase case:

$$\phi = \frac{\pi}{2} \rightarrow \omega_{out} = -\alpha k_d + k_c \tag{2.5}$$

19

labeled according to the relative phase shift, 0 or π. Depending of the sign of the backscattering parameters one of the solutions is stable and the other unstable, if $k_d > 0$ the *out of phase case* is stable, and the *in phase case* is stable for $k_d < 0$. The corresponding stationary solution for the carrier density N, as a function of the amplitude of the fields and the pump parameter, is

$$\bar{N} = \frac{\mu}{1 + 2Q^2(1 - sQ^2 - cQ^2)}. \tag{2.6}$$

For the amplitudes Q we find two solutions

In phase case:

$$Q_{in}^2 = \frac{1}{4(s+c)(1+k_d)}[2(k_d + 1) + \mu(s + c) -$$
$$-(4(k_d + 1)^2 + \mu^2(s + c)^2 - 4\mu(s + c)(1 + k_d) + 8(s + c)(1 - k_d^2))^{\frac{1}{2}}] \tag{2.7}$$

Out of phase case:

$$Q_{out}^2 = \frac{1}{4(s+c)(1-k_d)}[2(1 - k_d) + \mu(s + c) -$$
$$-(4(k_d - 1)^2 + \mu^2(s + c)^2 - 4\mu(s + c)(1 - k_d) - 8(s + c)(1 - k_d)(k_d - 1))^{\frac{1}{2}}]$$
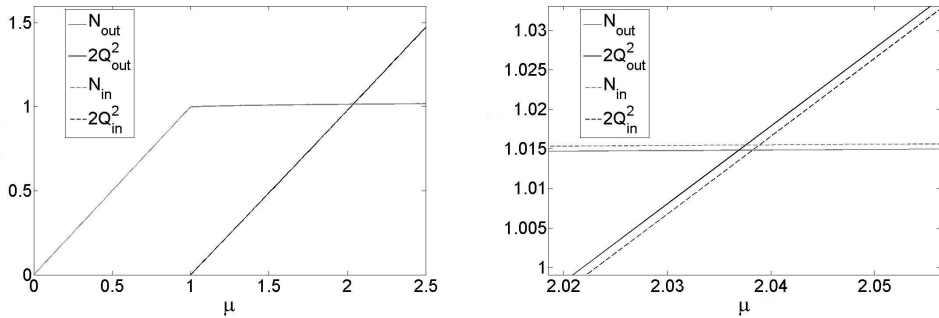$$\tag{2.8}$$

Figure 2.9: Stationary solutions versus the pump parameter.

In figure 2.9 the carrier inversion $\bar{N}$ and total intensity $2Q^2$ are plotted versus the pump parameter μ.

2.4   Linear fluctuations dynamics

In this section we analyse the effect of a perturbation on the above reported stationary solutions. We introduce a real perturbation $n(t)$ in the carrier density, and complex perturbations $a_\pm(t)$ for the fields

$$E_\pm(t) = (Q + a_\pm(t))e^{i\omega t \pm i\phi}$$
$$N(t) = \bar{N} + n(t). \qquad (2.9)$$

By making use of (2.9) in (2.1) we derive the following linear system for $n(t)$, $a_\pm(t)$ and $a_\pm^*(t)$

$$\begin{cases} \dot{n}(t) = -\gamma\{n(t) + [1 - 2Q^2(s+c)]\bar{N}Q(a_+(t) + a_+^*(t) + a_-(t) + a_-^*(t))+ \\ \qquad +2Q^2[1 - sQ^2 - cQ^2]n(t)\} \\ \dot{a}_\pm(t) = \frac{1}{2}(1 + i\alpha)\{\bar{N}(1 - sQ^2 - cQ^2)a_\pm(t) - \bar{N}Q^2[s(a_\pm(t) + a_\pm^*(t))+ \\ \qquad +c(a_\mp(t) + a_\mp^*(t))] + Q(1 - sQ^2 - cQ^2)n(t) - a_\pm(t)\}- \\ \qquad -i\omega a_\pm(t) - \eta(\cos 2\phi \mp i\sin 2\phi)a_\mp(t) + \xi_\pm(t) \\ \dot{a}_\pm^*(t) = \frac{1}{2}(1 - i\alpha)\{\bar{N}(1 - sQ^2 - cQ^2)a_\pm^*(t) - \bar{N}Q^2[s(a_\pm(t) + a_\pm^*(t))+ \\ \qquad +c(a_\mp(t) + a_\mp^*(t))] + Q(1 - sQ^2 - cQ^2)n(t) - a_\pm^*(t)\}+ \\ \qquad +i\omega a_\pm^*(t) - \eta^*(\cos 2\phi \pm i\sin 2\phi)a_\mp^*(t) + \xi_\pm^*(t) \end{cases} \qquad (2.10)$$

At this point we introduce a new set of variables, $S(t)$ and $R(t)$, to simplify our problem in two independent problems by block diagonalization. The new variables are

$$S(t) = a_+(t) + a_-(t)$$
$$R(t) = a_+(t) - a_-(t). \qquad (2.11)$$

$S(t)$ describes a perturbations to the total laser intensity and it is coupled to the carrier density perturbation equation. The variable $S(t)$ describes the perturbation of the total intensity of the lasers, regardless its distribution between the two modes. On the other side, $R(t)$ describes the power exchange between the two counter propagating fields. Those new variables are related to the $E_\pm(t)$ by

$$E_+(t) - E_-(t) \simeq ie^{i\omega_{out}t}(2Q + S(t)), \qquad (2.12)$$

$$E_+(t) + E_-(t) \simeq ie^{i\omega_{out}t}R(t) \qquad (2.13)$$

for the *out of phase case*, and by

$$E_+(t) + E_-(t) \simeq e^{i\omega_{in}t}(2Q + S(t)), \qquad (2.14)$$

$$E_+(t) - E_-(t) \simeq e^{i\omega_{in}t} R(t) \tag{2.15}$$

for the *in phase case.*

The equations for the dynamic evolution of $R(t)$ and $S(t)$ corresponding to each stationary solution are

In phase case:

$$\dot{S}_{in}(t) = (1 + i\alpha)\{Cn(t) + \widetilde{K}(S_{in}(t) + S_{in}^*(t))\} + \xi_S(t), \tag{2.16}$$

$$\dot{R}_{in}(t) = (1 + i\alpha)K(R_{in}(t) + R_{in}^*(t)) + 2\eta R_{in}(t) + \xi_R(t), \tag{2.17}$$

Out of phase case:

$$\dot{S}_{out}(t) = (1 + i\alpha)\{Cn(t) + \widetilde{K}(S_{out}(t) + S_{out}^*(t))\} + \xi_S(t), \tag{2.18}$$

$$\dot{R}_{out}(t) = (1 + i\alpha)K(R_{out}(t) + R_{out}^*(t)) - 2\eta R_{out}(t) + \xi_R(t), \tag{2.19}$$

where K, $\widetilde{K}$ and C are real constants defined by

$$\begin{aligned} K &= \tfrac{1}{2}\bar{N}Q^2(c - s) \\ \widetilde{K} &= -\tfrac{1}{2}\bar{N}Q^2(c + s) \\ C &= Q(1 - Q^2(c + s)). \end{aligned} \tag{2.20}$$

The carrier density perturbation equation is the same for both cases

$$\begin{aligned} \dot{n}(t) = -\gamma\{n(t) &+ [1 - 2Q^2(s + c)]\bar{N}Q(S(t) + S^*(t)) + \\ &+ 2Q^2[1 - sQ^2 - cQ^2]n(t)\}. \end{aligned} \tag{2.21}$$

Therefore we have two independent blocks. The block involving $R(t)$ and $R^*(t)$ describes the the relative intensity of the two counter propagating fields. On the other side, the block involving $S(t)$, $S^*(t)$ and $n(t)$ describes the total intensity of the fields and the perturbation in the carrier density.

2.5 Spectral correlations

Relative Intensity

The equations for the time evolution of $R_{out}(t)$ in matrix form are

$$\begin{pmatrix} \dot{R}_{out}(t) \\ \dot{R}^*_{out}(t) \end{pmatrix} = \begin{pmatrix} (1+i\alpha)K - 2\eta & (1+i\alpha)K \\ (1-i\alpha)K & (1-i\alpha)K - 2\eta^* \end{pmatrix} \begin{pmatrix} R_{out}(t) \\ R^*_{out}(t) \end{pmatrix} + \begin{pmatrix} \xi_R(t) \\ \xi^*_R(t) \end{pmatrix}. \tag{2.22}$$

The corresponding eigenvalues are

$$\lambda^{out}_{1,2} = K - 2k_d \pm [K^2 + 4K\alpha k_c - 4k_c^2]^{\frac{1}{2}} \tag{2.23}$$

for the *out of phase case*, whereas for the *in phase case* the system is

$$\begin{pmatrix} \dot{R}_{in}(t) \\ \dot{R}^*_{in}(t) \end{pmatrix} = \begin{pmatrix} (1+i\alpha)K + 2\eta & (1+i\alpha)K \\ (1-i\alpha)K & (1-i\alpha)K + 2\eta^* \end{pmatrix} \begin{pmatrix} R_{in}(t) \\ R^*_{in}(t) \end{pmatrix} + \begin{pmatrix} \xi_R(t) \\ \xi^*_R(t) \end{pmatrix}, \tag{2.24}$$

and the eigenvalues are

$$\lambda^{in}_{1,2} = K + 2k_d \pm [K^2 - 4K\alpha k_c - 4k_c^2]^{\frac{1}{2}}. \tag{2.25}$$

From now on we focus on the *out of phase case*, because we have chosen the parameters set in which such solution is stable. And we set the noise amplitude D equal to 10^{-7}.

We apply the Fourier transform to the $R_{out}(t)$ and $R^*_{out}(t)$ differential equations, by taking the following definition of Fourier transform

$$\widetilde{f}(\omega) = \int_{-\infty}^{\infty} f(t)e^{-i\omega t}dt \qquad f(t) = \frac{1}{2\pi}\int_{-\infty}^{\infty} \widetilde{f}(\omega)e^{i\omega t}d\omega \tag{2.26}$$

yielding

$$\begin{cases} i\omega \widetilde{R}_{out}(\omega) = K(1+i\alpha)[\widetilde{R}_{out}(\omega) + \widetilde{R}^*_{out}(-\omega)] - 2\eta\widetilde{R}_{out}(\omega) + \widetilde{\xi}_R(\omega) \\ i\omega \widetilde{R}^*_{out}(-\omega) = K(1-i\alpha)[\widetilde{R}_{out}(\omega) + \widetilde{R}^*_{out}(-\omega)] - 2\eta^*\widetilde{R}^*_{out}(-\omega) + \widetilde{\xi}^*_R(-\omega) \end{cases}. \tag{2.27}$$

The analytical solution of the above system is

$$\widetilde{R}_{out}(\omega) = \frac{1}{A(\omega)}[(i\omega - (1-i\alpha)K + 2\eta^*)\widetilde{\xi}_R(\omega) + (1+i\alpha)K\widetilde{\xi}^*_R(-\omega)] \tag{2.28}$$
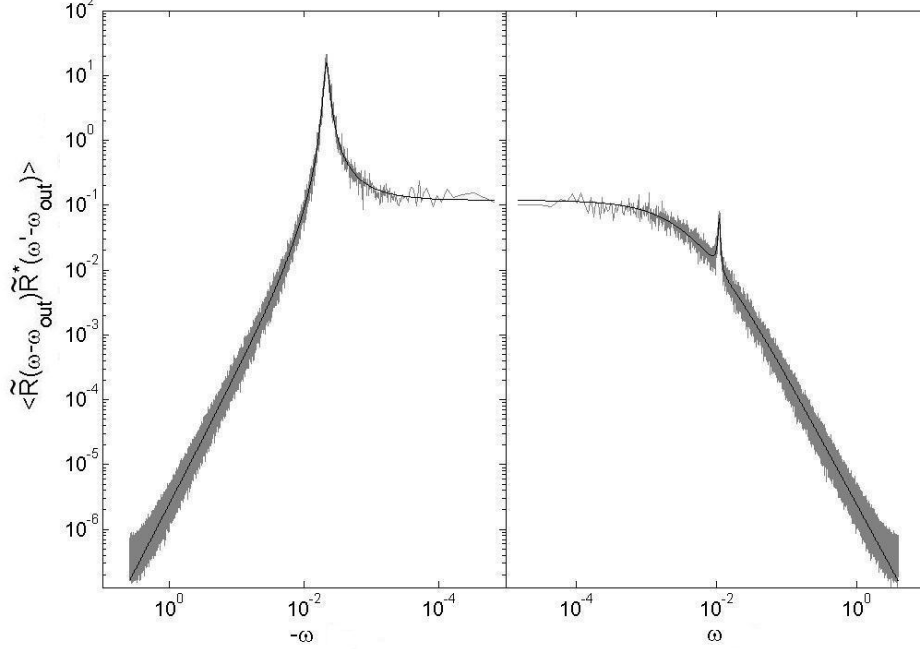
Figure 2.10: $< (\widetilde{E}_+(\omega) + \widetilde{E}_-(\omega))(\widetilde{E}_+(\omega') + \widetilde{E}_-(\omega'))^* > = < \widetilde{R}(\omega - \omega_{out})\widetilde{R}^*(\omega' - \omega_{out}) >$ spectrum, the grey line corresponds to the numerical simulation, the analytical solution is the black line.

$$\widetilde{R}_{out}^*(\omega) = \frac{1}{A(-\omega)}[(1 - i\alpha)K\widetilde{\xi}_R(-\omega) + (2\eta - i\omega - (1 + i\alpha)K)\widetilde{\xi}_R^*(\omega)] \quad (2.29)$$

where

$$A(\omega) = -\omega^2 + i\omega(4k_d - 2K) - 4(k_d + \alpha k_c)K + 4(k_d^2 + k_c^2).$$

Taking profit of the statistical properties of the spontaneous emission noise for the fields (2.2), we find the properties of the noise sources for the system $\widetilde{R}(\omega)$ (2.27),

$$\langle \widetilde{\xi}_R(\omega)\widetilde{\xi}_R^*(\omega') \rangle = 8\pi D\delta(\omega - \omega'). \quad (2.30)$$

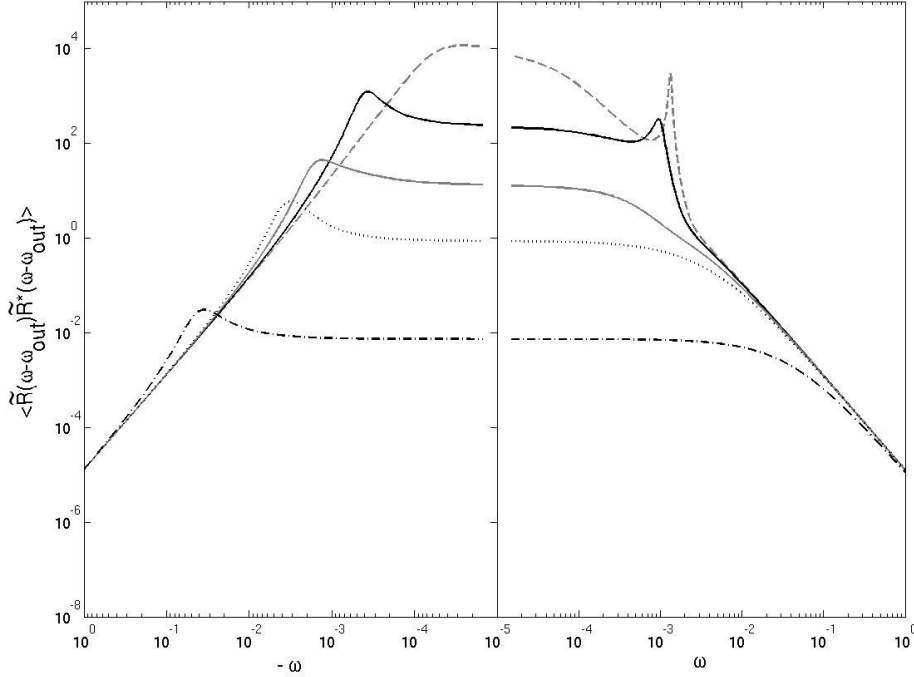By making use of (2.30) we find an analytical expression for the ensemble average

24

Figure 2.11: $< \widetilde{R}(\omega - \omega_{out})\widetilde{R}^*(\omega' - \omega_{out}) >$ spectrum dependence on dissipative backscattering coefficient, k_d, versus the dimensionless frequency, ω. The dashed grey curve corresponds to $k_d = 10^{-4}$, the black to $k_d = 2\ 10^{-4}$, the grey to $k_d = 5\ 10^{-4}$, the dotted black to $k_d = 10^{-3}$ and the dash-dotted black line to $k_d = 10^{-2}$. ($k_c = 10^{-3}$ and $\mu = 1.2$)

$$\langle \widetilde{R}_{out}(\omega)\widetilde{R}^*_{out}(\omega') \rangle = \frac{1}{A(\omega)A(-\omega)}[4k_d^2 - 4K(k_d + k_c\alpha) + 2K^2(1 + \alpha^2) + \\ +2K\alpha\omega + (\omega - 2k_c)^2]8\pi D\delta(\omega - \omega').$$

$$(2.31)$$

Figure 2.10 shows a comparison between the analytical expression (2.31) and numerical simulations for 20 realizations. The agreement between the analytical and the numerical solutions is very good at all frequencies.

Figure 2.11 shows the spectral dependence on dissipative backscattering coefficient k_d. The resonance peak moves towards negatives frequencies for higher values of k_d. The spectrum dependence on the conservative coefficient k_c, is shown in the figure 2.12. In the figure 2.13 the spectrum dependence
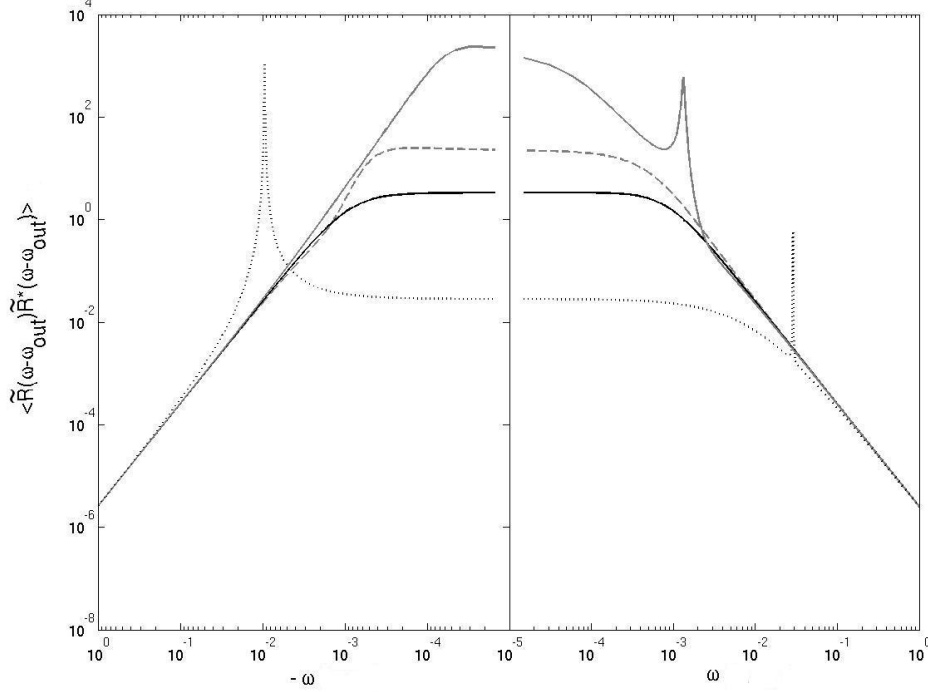
Figure 2.12: $< \widetilde{R}(\omega - \omega_{out})\widetilde{R}^*(\omega' - \omega_{out}) >$ spectrum dependence on conservative backscattering coefficient, k_c, versus the dimensionless frequency, ω. The dashed grey curve corresponds to $k_c = 10^{-4}$, the black to $k_c = 5\ 10^{-4}$, the grey to $k_c = 10^{-3}$ and dotted black to $k_c = 10^{-2}$. ($k_d = 10^{-4}$ and $\mu = 1.2$)

on pump parameter, μ, is shown.

Total intensity and carrier density

The system describing $S(t)$ and $n(t)$ can be put in matrix form, yielding for the *out of phase case*,

$$
\begin{pmatrix} \dot{S}_{out}(t) \\ \dot{S}^*_{out}(t) \\ \dot{n}_{out}(t) \end{pmatrix} = \begin{pmatrix} (1+i\alpha)\widetilde{K} & (1+i\alpha)\widetilde{K} & (1+i\alpha)C \\ (1-i\alpha)\widetilde{K} & (1-i\alpha)\widetilde{K} & (1-i\alpha)C \\ -\gamma(2Q\widetilde{K}+\bar{N}C) & -\gamma(2Q\widetilde{K}+\bar{N}C) & -\gamma(1+2QC) \end{pmatrix} \begin{pmatrix} S_{out}(t) \\ S^*_{out}(t) \\ n_{out}(t) \end{pmatrix} + \begin{pmatrix} \xi_S(t) \\ \xi^*_S(t) \\ 0 \end{pmatrix}.
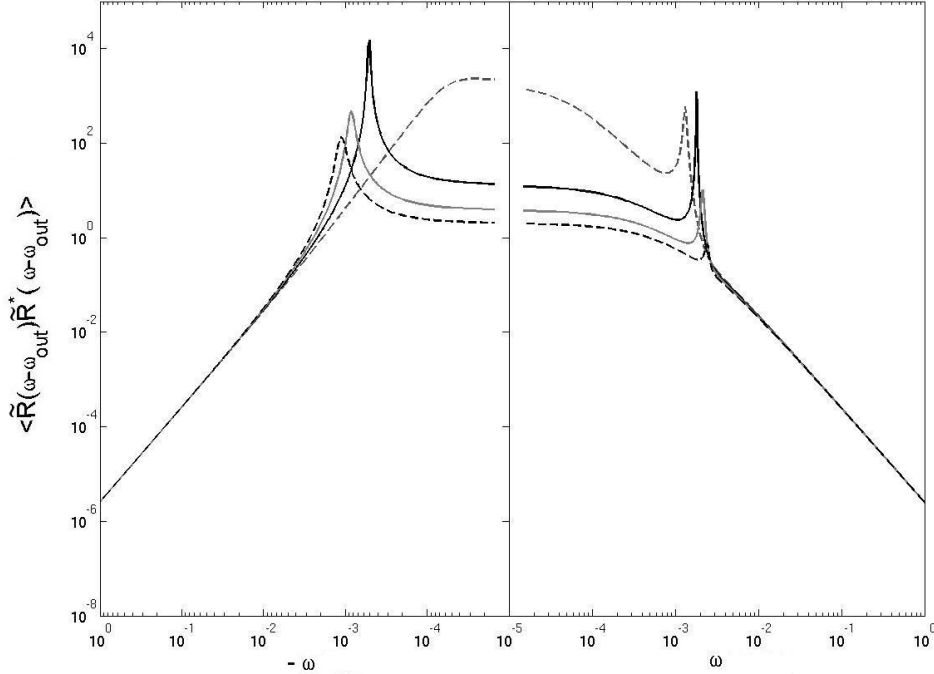$$

$$(2.32)$$

Figure 2.13: $< \widetilde{R}(\omega - \omega_{out})\widetilde{R}^*(\omega' - \omega_{out}) >$ spectrum dependence on pump current, μ, versus the dimensionless frequency, ω. The dashed grey curve corresponds to $\mu = 1.2$, the black to $\mu = 1.15$, the grey to $\mu = 1.1$ and the dashed black to $\mu = 1.05$. ($k_c = 10^{-3}$ and $k_d = 10^{-4}$)

As we did for the $R(t)$ system, we find the eigenvalues of the matrix

$$\lambda_0^{out} = 0,$$
$$\lambda_{1,2}^{out} = \widetilde{K} - \tfrac{\gamma}{2} - \gamma QC \pm \tfrac{1}{2}[\gamma^2 + 4(\widetilde{K}^2 + \widetilde{K}\gamma + \gamma^2 QC(1 + QC)) - 8\gamma(\widetilde{K}QC + nC^2)]^{\frac{1}{2}}.$$
(2.33)

In this case we find the presence of a zero eigenvalue, λ_0^{out}, which indicates that the matrix is singular. If we use (2.26) and apply the fourier transform to the system describing $S(t)$ and $n(t)$ we find

$$\begin{cases} i\omega\widetilde{S}(\omega) = (1 + i\alpha)\widetilde{K}[\widetilde{S}(\omega) + \widetilde{S}^*(-\omega)] + (1 + i\alpha)C\widetilde{n}(\omega) + \widetilde{\xi}_S(\omega) \\ i\omega\widetilde{S}^*(-\omega) = (1 - i\alpha)\widetilde{K}[\widetilde{S}(\omega) + \widetilde{S}^*(-\omega)] + (1 - i\alpha)C\widetilde{n}(\omega) + \widetilde{\xi}_S^*(-\omega) \\ i\omega\widetilde{n}(\omega) = -\gamma(2Q\widetilde{K} + \bar{N}C)[\widetilde{S}(\omega) + \widetilde{S}^*(-\omega)] - \gamma(1 + 2QC)\widetilde{n}(\omega) \end{cases} .$$
(2.34)

27

We solve the above system in the Fourier space, leading to an analytical expressions for $\widetilde{S}(\omega)$, $\widetilde{S}^*(\omega)$ and $\widetilde{n}(\omega)$,

$$\widetilde{S}(\omega) = \tfrac{1}{B(\omega)}[(-\omega^2 + i\omega(\gamma(1+2QC)-(1-i\alpha)\widetilde{K})+(1-i\alpha)\gamma(C^2\bar{N}-\widetilde{K}))\widetilde{\xi}_S(\omega)+$$
$$+(1+i\alpha)(i\omega\widetilde{K}+\gamma(\widetilde{K}-C^2\bar{N}))\widetilde{\xi}_S^*(-\omega)], \tag{2.35}$$

$$\widetilde{S}^*(\omega) = \tfrac{1}{B(-\omega)}[(-\omega^2 - i\omega(\gamma(1+2QC)-(1+i\alpha)\widetilde{K})+(1+i\alpha)\gamma(C^2\bar{N}-\widetilde{K}))\widetilde{\xi}_S^*(\omega)+$$
$$+(1-i\alpha)(-i\omega\widetilde{K}+\gamma(\widetilde{K}-C^2\bar{N}))\widetilde{\xi}_S(-\omega)], \tag{2.36}$$

and

$$\widetilde{n}(\omega) = \frac{1}{B(\omega)}[-i\omega\gamma(2Q\widetilde{K}+\bar{N}C)](\widetilde{\xi}_S(\omega)+\widetilde{\xi}_S^*(-\omega)), \tag{2.37}$$

where

$$B(\omega) = -i\omega^3 - \omega^2[\gamma(1+2QC)-2\widetilde{K}] - 2i\omega\gamma(\widetilde{K}-\bar{N}C^2).$$

Taking profit of the statistical properties (2.2) of the noise sources and the definition of $S(t)$ we are able to characterize $\xi_S(t)$ by its statistical properties in the Fourier space,

$$\langle\widetilde{\xi}_S(\omega)\widetilde{\xi}_S^*(\omega')\rangle = 8\pi D\delta(\omega-\omega'). \tag{2.38}$$

By using this properties and the solutions $\widetilde{S}(\omega)$ of the system (2.35) and (2.36) we find following ensemble average

$$\langle\widetilde{S}(\omega)\widetilde{S}^*(\omega')\rangle = \tfrac{1}{B(\omega)B(-\omega)}\{\omega^4 - \omega^3 2\widetilde{K}\alpha + \omega^2[\gamma^2(1+2QC)^2 + 2(1+\alpha^2)\widetilde{K}^2 +$$
$$+\gamma^2(\widetilde{K}-C^2\bar{N})^2 - 2\gamma\widetilde{K}(1+2QC) - 2\gamma(C^2\bar{N}-\widetilde{K})]-$$
$$-2\omega\alpha\gamma^2(C^2\bar{N}-\widetilde{K})(1+2QC)]\}8\pi D\delta(\omega-\omega'). \tag{2.39}$$

However, the presence of a zero eigenvalue λ_0^{out} makes the linear analysis more complicated respect to the previous case. Indeed, the imaginary part of $S(t)$, $\mathbb{I}m(S(t))$ which corresponds to the eigenvector, $v_0^{out} = S(t) - S^*(t)$, associated to λ_0^{out}, changes dizzy in an undamped fashion as can be seen in figure 2.15, therefore the linearization is not strictly valid. This effect is known in the literature as Goldstone mode.

In general we can consider a set of fields $x_i(t)$ which obey dynamical equations of the form
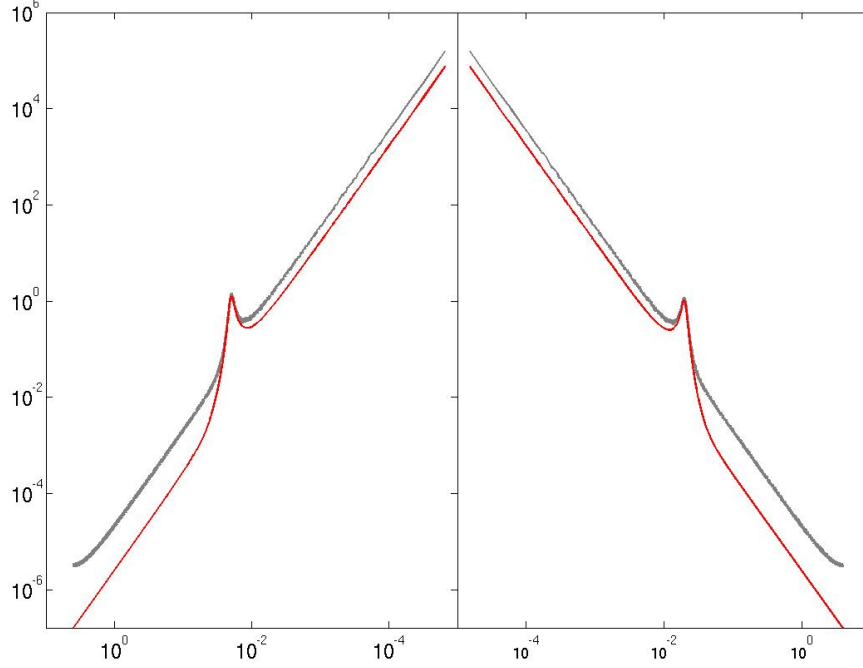
Figure 2.14: $< \widetilde{S}(\omega)\widetilde{S}^*(\omega) >$ spectrum versus dimensionless frequency ω. The grey curve corresponds to the numerical simulation and the black to the analytical solution.

$$\frac{\partial x_i(t)}{\partial t} = F_i(x_1, \ldots, x_N), \qquad (2.40)$$

where F_i is a general function of the fields $x_i(t)$, and such that they admit a stationary solution x_i^0. The linear analysis of fluctuations around this solution configuration is made by calculating the eigenvalues of the matrix

$$M_{l\ k} = \frac{\partial F_l}{\partial x_k}\big|_{x_i=x_i^0}. \qquad (2.41)$$

In optics, propagating fields presents phase invariance, i.e. a propagating field, solution of a wave equation, can be written as $x_i^0 = x_i e^{i\phi}$, where ϕ is an arbitrary global phase. As a consequence of such phase invariance, the dynamic evolution of the field shows a invariant direction in the phase space (e.g. a zero eigenvalue is found). In presence of noise, such invariant direction (Goldstone mode) shows undamped fluctuations. As a further consequence,

a theoretical linearized analysis must carefully treat such problem, indeed a linear analysis is valid in a subspace orthogonal to the eigenvector associated to the zero eigenvalue.
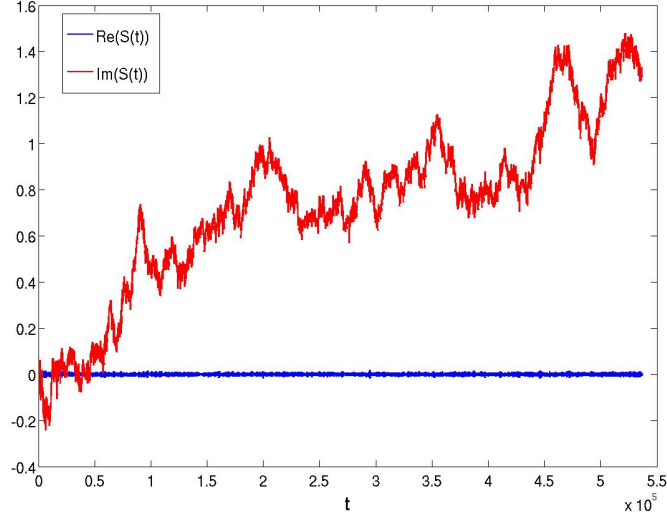

Figure 2.15: Temporal evolution of $\mathbb{R}e(S(t))$, in black, and $\mathbb{I}m(S(t))$ in grey.

To get rid of the Goldstone mode, we use a new variable associated to the real part of $S(t)$, which is orthogonal to v_0^{out},

$$P(t) = S(t) + S^*(t) = 2\mathbb{R}e(S(t)), \tag{2.42}$$

which obeys to the following system of differential equations

$$\begin{cases} \dot{P}(t) = 2\widetilde{K}P(t) + 2Cn(t) + \xi_P(t) \\ \dot{n}(t) = -\gamma(2Q\widetilde{K} + \bar{N}C)P(t) - \gamma(1 + 2QC)n(t) \end{cases}. \tag{2.43}$$

Again by using Fourier transform, we derive a system of linear equations for $\widetilde{P}(\omega)$ and $\widetilde{n}(\omega)$, yielding

$$\begin{cases} i\omega\widetilde{P}(\omega) = 2\widetilde{K}\widetilde{P}(\omega) + 2C\widetilde{n}(\omega) + \widetilde{\xi}_P(\omega) \\ i\omega\widetilde{n}(\omega) = -\gamma(2Q\widetilde{K} + \bar{N}C)\widetilde{P}(\omega) - \gamma(1 + 2QC)\widetilde{n}(\omega) \end{cases}, \tag{2.44}$$

solved by

$$\widetilde{P}(\omega) = \frac{1}{\widetilde{B}(\omega)}[i\omega + \gamma(1 + 2QC)]\widetilde{\xi}_P(\omega) \qquad (2.45)$$

and

$$\widetilde{n}(\omega) = \frac{-1}{\widetilde{B}(\omega)}\gamma(2Q\widetilde{K} + \bar{N}C)\widetilde{\xi}_P(\omega), \qquad (2.46)$$

where

$$\widetilde{B}(\omega) = -\omega^2 + i\omega[\gamma(1 + 2QC) - 2\widetilde{K}] + 2\gamma(C^2\bar{N} - \widetilde{K}). \qquad (2.47)$$

As we did before we find the statistical properties of the noise for $\widetilde{P}(\omega)$,

$$\langle\widetilde{\xi}_P(\omega)\widetilde{\xi}_P^*(\omega')\rangle = 16\pi D\delta(\omega - \omega'), \qquad (2.48)$$

and we are able to find the following ensemble average

$$< \widetilde{P}(\omega)\widetilde{P}^*(\omega') >= \frac{1}{\widetilde{B}(\omega)\widetilde{B}^*(\omega)}[\omega^2 + \gamma^2(1 + 2QC)^2]16\pi D\delta(\omega - \omega'). \quad (2.49)$$

Figure 2.16 shows a comparison between the analytical expression (2.49) and numerical simulations. The agreement between numerical (20 realizations) and analytical solutions is very good.

Figure 2.17 shows analytical spectra for different pump current values. For increasing pump current values the peaks splits more.
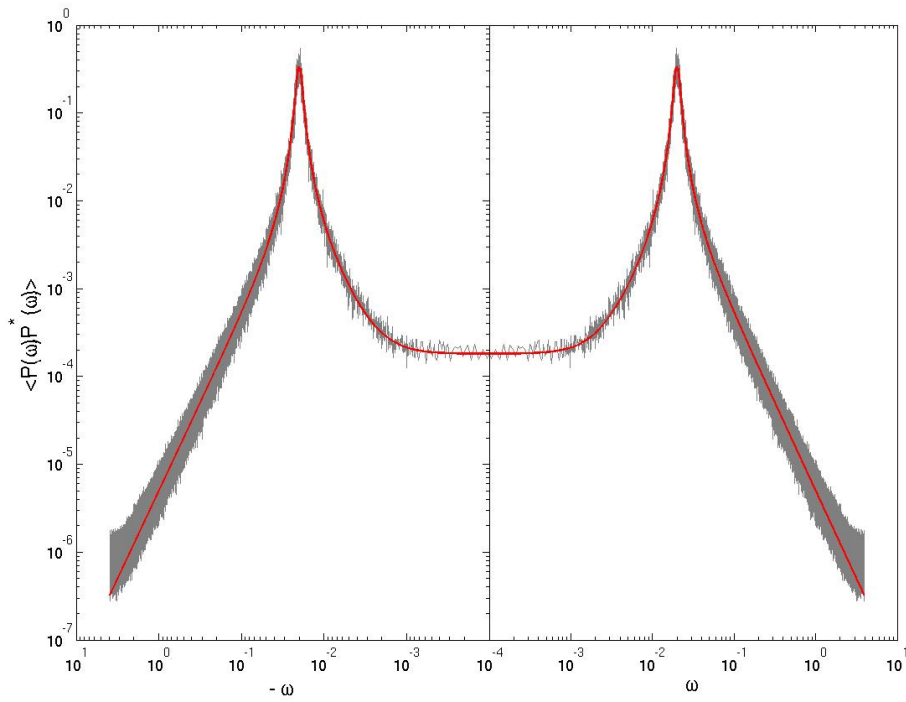
Figure 2.16: $< \widetilde{P}(\omega)\widetilde{P}^*(\omega) >$ versus dimensionless frequency, ω. The grey line corresponds to the numerical simulation and the black line is the analytical solution (2.49).
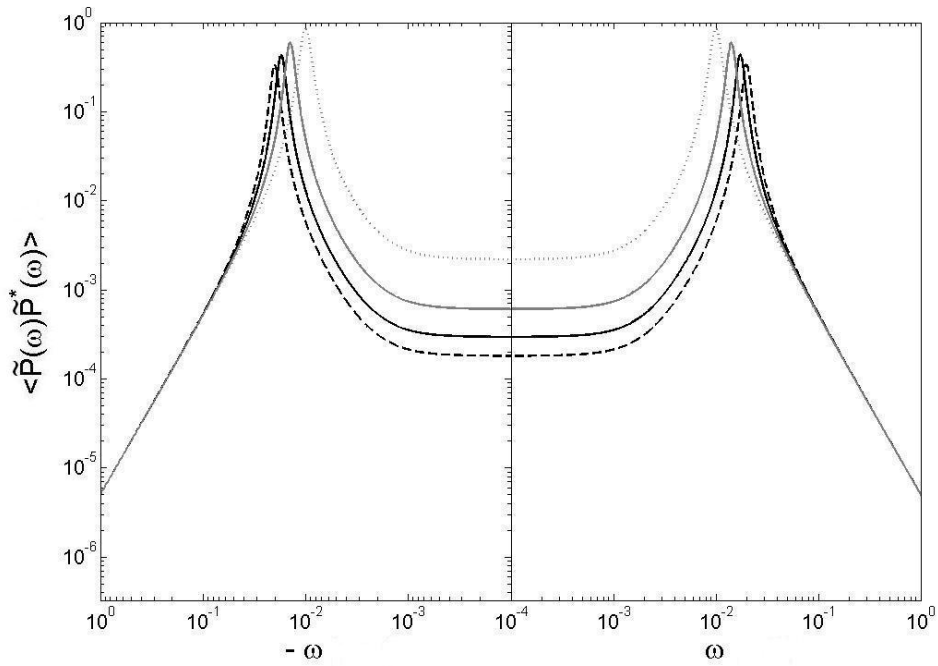
Figure 2.17: $< \widetilde{P}(\omega)\widetilde{P}^*(\omega) >$ spectral dependence on the pump parameter, μ, versus dimensionless frequency ω. The dashed black curve corresponds to $\mu = 1.2$, the black to $\mu = 1.15$, the grey to $\mu = 1.1$ and the dotted grey to $\mu = 1.05$.

Chapter 3

Conclusions and future work

We have studied the influence of spontaneous emission noise in a two-mode model for semiconductor ring lasers, biased in the bidirectional static emission regime. The analysis has been carried out by linearizing the model close to a stable stationary solution, and considering effect of noise as stochastic perturbations expressed by Langevin forces. At a linear level, pertubations concerning the total intensity and carrier inversion dynamics decouple from the energy distribution processes between the two modes. This fact permitted a full analytic analysis, well confirmed by numerical simulations of the complete non linear system. The analysis showed that semiconductor ring lasers have peculiar noise properties. On one side the total intensity and carrier density show a noise spectrum characterized by a resonance induced by the typical field-medium exchange processes (relaxation oscillations) and the global phase invariance induced by the Goldstone mode, so as far as those variables are concerned, it behaves as a standard single-mode Fabry-Perot semiconductor laser. Besides, the degree of freedom associated to the simultaneous presence of two counterpropagating modes allows for a further process of energy exchange *between* the two modes. Our analysis unveiled that such process presents a resonance peak as well, influenced mainly by the backscattering parameters, and can be excited in the bidirectional regime as a 'noisy precursor' of a Hopf bifurcation.

The present work represents the development of reliable tools for the simulation and analytical analysis of a model for semiconductor ring lasers. Reliability has been tested by a thoughout comparison between simulation and calculations. Future developments will range from quantitative evaluation of two-times correlations functions, to applications to rotation sensing, to analysis of the stochastic jumps induced by noise in the bistable regime.

Appendix A

Heun's algorithm

The Heun's algorithm is a method to solve stochastic differential equations (SDE) based on the order two Runge-Kutta method for ordinary differential equations (ODE). A generic SDE has the following expression for a dynamical variable $x(t)$:

$$\dot{x}(t) = q(x, t) + g(t, x)\xi_w(t)$$

where $q(x, t)$ and $g(x, t)$ are functions, linear or non linear, and $\xi_w(t)$ is a white gaussian noise, which properties are

$$\langle \xi_w(t)\xi_w(t') \rangle = 2D\delta(t - t')$$

A possible algorithm [15] to solve the SDE is

$$k = hq(t, x(t))$$
$$l = h^{1/2}u(t)g(t, x(t))$$
$$x(t + h) = x(t) + \frac{h}{2}[q(t, x(t)) + q(t + h, x(t) + l + k)] +$$
$$+ \frac{1}{2}h^{1/2}u(t)[g(t, x(t)) + g(t + h, x(t) + k + l)]$$

where h is the temporal step and $u(t)$ is a independent set of random gaussian numbers with zero mean value and variance equal to one.

Appendix B

Semiconductor ring laser gyroscope responsivity

A possible application of an SRL is in the field of inertial rotation sensing. A SRL Gyroscope (S-RLG) would represent a compact, simple and low cost optical gyroscope. All the RLGs are based on the measure of the detuning induced by the rotation on the optical frequency of the two counterpropagating modes in a Ring Laser. However, the unavoidable backscattering effects couple and lock the counterpropagating waves, representing a major source of error in real devices [3]. In the following, we theoretically show how a SRL can be used to measure inertial rotation within the so called *locking-band*, i.e. without the need to un-lock the two counterpropagating waves. We provide an analytical expression for the Responsivity.

In the figure 1.2 (c) we see the effect of mode locking in the behavior of the beat frequency, f, depending on the rotation rate, Ω, which corresponds to the solutions of equation (1.5) reported in (1.6). In the locking range, the frequency difference vanishes but we can obtain information about the phase difference (1.6), using the fact that we are dealing with a semiconductor laser, where the phase and amplitude are coupled by the α factor, so we analyze the effect of a detuning induced by an inertial rotation over the fields amplitudes.

Consistently with the standard theory [3], the emission frequency of the two modes (referred to a common optical carrier set to zero) is shifted by the inertial rotation of an amount equal to 2Δ, when the rotation vector is orthogonal to the cavity plane,

$$\Delta = \frac{2\pi R \tau_p}{\lambda} \Omega_{rot} \,, \qquad (B.1)$$

where R is the ring radius, λ is the laser wavelength, and Ω_{rot} is the rotation angular velocity. The way to introduce the rotation to the rate equations (1.13) is by adding the detuning term (B.1) in the equations for the fields

$$\begin{cases} \dot{E}_\pm(t) = \mathcal{G}_\pm(N(t), |E_\pm(t)|^2) \, E_\pm(t) - \eta \, E_\mp(t) \pm i\Delta E_\pm(t) \\ \dot{N}(t) = \gamma \, \mathcal{F}(N(t), |E_\pm(t)|^2) \end{cases} . \qquad (B.2)$$

In this case we suppose that the two counter-propagating fields have different amplitudes, therefore we substitute in the set (B.2) a solution of the following form

$$E_\pm(t) = Q_\pm e^{i\omega_\pm t \pm i\phi_\pm}. \qquad (B.3)$$

We make use of (B.3) in the equations for the electric fields (B.2), assuming $\omega_+ = \omega_- = \omega$, and separating the real part and the imaginary part, we obtain

$$\begin{cases} \frac{1}{2}[N(t)(1 - sQ_\pm^2 - cQ_\mp^2) - 1]Q_\pm - k_d Q_\mp \cos\phi \mp k_c Q_\mp \sin\phi = 0 \\ \omega Q_\pm = \frac{\alpha}{2}[N(t)(1 - sQ_\pm^2 - cQ_\mp^2) - 1]Q_\pm - k_c Q_\mp \cos\phi \pm k_d Q_\mp \sin\phi \pm \Delta Q_\pm \end{cases} \\ (B.4)$$

At this point we make use the value for the stationary solutions with Q (2.7) to relate with the amplitude $Q_\pm$, by considering a small symmetric deviation, δ, in the following way

$$Q_\pm = Q \pm \delta, \qquad (B.5)$$

and a small deviation θ of the relative phase

$$\psi = 2\phi + \theta, \qquad (B.6)$$

by substituting eq. (B.5) in eq.(B.4), at first order in δ and θ, for the *in phase case* we obtain

$$\begin{cases} \frac{1}{2}[N(t)(1 - s(Q^2 \pm 2Q\delta) - c(Q^2 \mp 2Q\delta)) - 1](Q \pm \delta) - (k_d \pm k_c\theta)(Q \mp \delta) = 0 \\ \omega(Q \pm \delta) = \frac{\alpha}{2}[N(t)(1 - s(Q^2 \pm 2Q\delta) - c(Q^2 \mp 2Q\delta)) - 1](Q \pm \delta) - \\ -(k_c \mp k_d\theta)(Q \mp \delta) \pm \Delta(Q \pm \delta) \end{cases} \\ (B.7)$$

as a check, the order zero (i.e. $\Delta = \delta = \theta = 0$) of the above system leads back to the unperturbed solution (2.4)

$$\omega = \omega_{in} = \alpha k_d - k_c \qquad (B.8)$$

the second linear equation for the deviations θ and δ is

$$\Delta Q + \theta Q(\alpha k_c + k_d) - 2(\alpha k_d - k_c)\delta = 0, \tag{B.9}$$

which can be solved in terms of the other parameters

$$\theta = \frac{2(\alpha k_d - k_c)\delta}{(\alpha k_c + k_d)Q} - \frac{\Delta}{\alpha k_c + k_d} \tag{B.10}$$

by making use of the stationary solutions (2.6, 2.7 and B.8) in (B.7), we arrive to

$$\begin{cases} \Delta Q + k_d\theta Q + 2k_c\delta - 2\alpha Q^2\delta\bar{N}(s-c) = 0 \\ 2k_d\delta - k_c\theta Q - \bar{N}Q^2\delta(s-c) = 0 \end{cases} \tag{B.11}$$

finally we find an expression for δ depending on Δ:

$$\delta = -[\frac{k_d}{k_c Q}(2k_d - \bar{N}Q^2(s-c)) + \frac{2}{Q}(k_c - \alpha Q^2\bar{N}(s-c))]^{-1}\Delta \tag{B.12}$$

we define χ as the difference between the fields intensities divided by the total intensity,

$$\chi = \frac{|E_+|^2 - |E_-|^2}{|E_+|^2 + |E_-|^2} = \frac{2}{Q}\delta = \mathcal{R}\Omega_{rot} \tag{B.13}$$

where $\mathcal{R}$ is the responsivity of the system to the inertial rotation.

Therefore, the responsivity $\mathcal{R}$ can be written as

$$\mathcal{R} = \frac{2}{Q}[\frac{k_d}{k_c Q}(2k_d - \bar{N}Q^2(s-c)) + \frac{2}{Q}(k_c - \alpha Q^2\bar{N}(s-c))]^{-1}\frac{2\pi R\tau_p}{\lambda} . \tag{B.14}$$

In figure B.1 the difference between the fields intensities divided by the total intensity, χ, is plotted versus the inertial rotation Ω_{rot}.

Figure B.2 shows responsivity versus conservative backscattering coefficient, k_c for different values of dissipative backscattering coefficient, k_d. A more detailed plot of responsivity versus the backscattering coefficients is shown in figure B.3.

Figure B.4 shows responsivity versus pump current, there is a maximum responsivity for the pump value near 1.12.
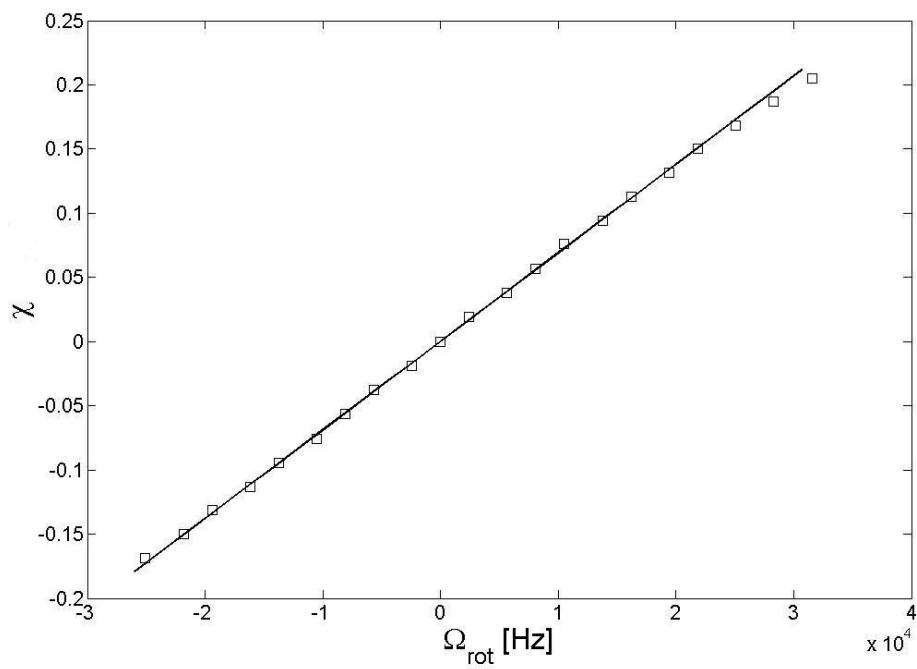
Figure B.1: Difference between the fields intensities divided by the total intensity χ, versus inertial rotation Ω_{rot}. The black line correspond to the analytical expression (B.13) and the squares to the numerical simulation. The slope is the responsivity $\mathcal{R}$.
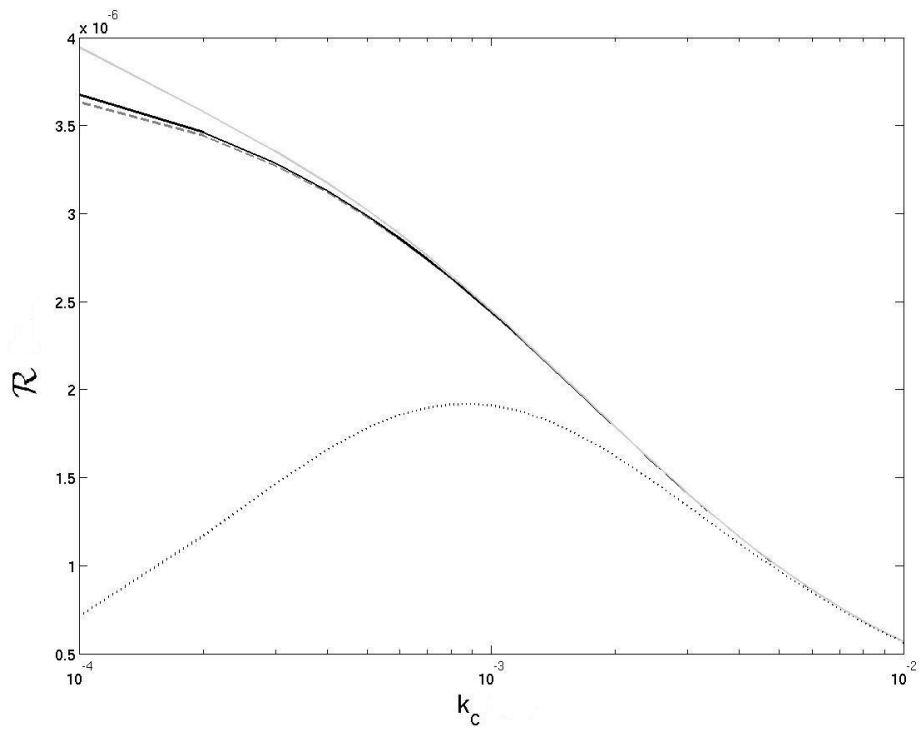
Figure B.2: Responsivity versus conservative backscattering coefficient, k_c. The grey dashed curve corresponds to $k_d = 10^{-6}$, the black to $k_d = 10^{-5}$, the grey to $k_d = 10^{-4}$ and the dotted black to $k_d = 10^{-3}$. $\mu = 1.2$.
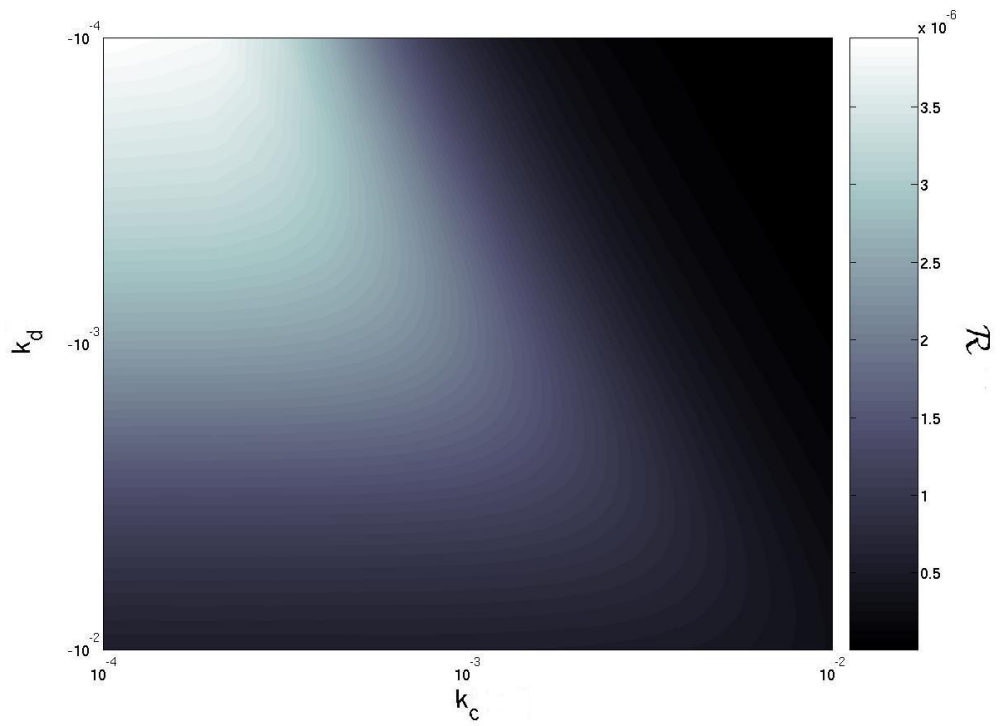
Figure B.3: Responsivity versus backscattering coefficients. $\mu = 1.2$.
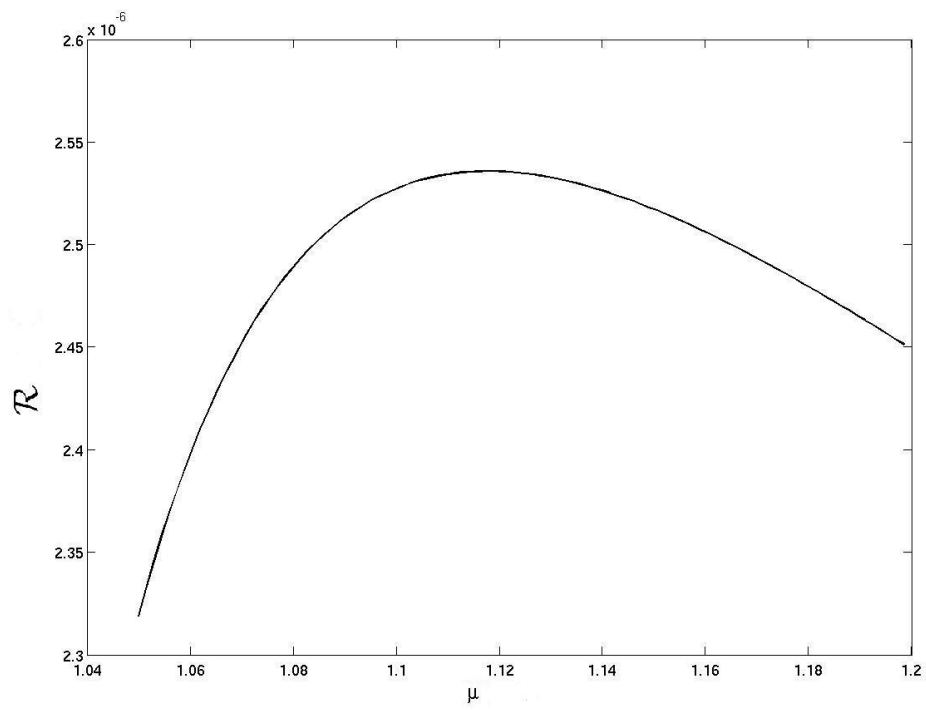
Figure B.4: Responsivity versus pump parameter, μ. $k_d = -10^{-4}$ and $k_c = 10^{-3}$.

Bibliography

[1] C.H. Rowe,U.K. Schreiber, S.J. Cooper, B.T. King, M. Poulton and G.E. Stedman, *Design and operation of a very large ring laser gyroscope*, Applied Optics, vol. 38, no. 12, 20 April 1999.

[2] K. Taguchi, K. Fukushima, A. Ishitani and M. Ikeda, *Optical inertial rotation sensor using semiconductor ring laser*, Electronics Letters, vol. 34, no. 18, p. 1775, 3 September 1998.

[3] W.W. Chow, J. Gea-Banacloche, L.M. Pedrotti, V.E. Sanders, W. Schleich and M.O. Scully, *The ring laser gyro*, Reviews of Modern Physics, vol. 57, no.1, January 1985.

[4] A.S.H. Liao and S. Wang, *Semiconductor injetion lasers with circular resonator*, Applied Physics Letters, vol. 36, no. 10, 15 May 1980.

[5] T.F. Krauss, R.M. De La Rue and P.J.R Laybourn, *Impact of output coupler configuration on operating characteristics of semiconductor ring lasers*, Journal of Lightwave Technology, vol. 13, no. 17, July 1995.

[6] H. Han, D.V. Forbes and J.J. Coleman, *InGaAs-AlGaAs-GaAs strained-layer quantum-well heterostructure square ring lasers*, IEEE Journal of Quantum Electronics, vol. 31, no. 11, p. 1994, November 1995.

[7] C. Ji, M.H. Leary and J.M. Ballantyne, *Long-wavelength triangular ring laser*, IEEE Photonics Technology Letters, vol. 9, no. 11, p. 1469, November 1997.

[8] G. Griffel, J.H. Abeles, R.J. Menna, A.M. Braun, J.C. Connolly and M. King, *Low-threshold InGaAsP ring lasers fabricated using bi-level dry etching.*, IEEE Photonics Technology Letters, vol. 12, no. 2, p. 146, February 2002.

[9] L. Bach, J.P. Reithmaier, A. Forchel, J.L. Gentner and L. Goldstein, *Wavelength stabilized single-mode lasers by coupled micro-square resonators*, IEEE Photonics Technology Letters, vol. 15, no. 3, p. 377, March 2003.

[10] H. Cao, H. Ling, C. Liu, H. Deng, M. Benavidez, V.A. Smagley, R.B. Caldwell, G.M. Peake, G.A. Smolyakov, P.G. Eliseev and M. Osinski, *Large S-section-ring-cavity diode lasers: Directional switching, electrical diagnostics, and mode beating spectra*, IEEE Photonics Technology Letters, vol. 17, no. 2, p. 282, February 2005.

[11] M. Sorel, G. Giuliani, A. Scirè, R. Miglieria, S. Donati and P.J.R. Laybourn, *Operating regimes of GaAs-AlGaAs semiconductor ring lasers: Experiment and model*, IEEE Journal of Quantum Electronics, vol. 39, no. 10, p. 1187, October 2003.

[12] M.T. Hill, H.J.S. Dorren, T.de Vrie, X.J.M. Leijtens, J.H. den Besten, B. Smalbrugge, Y.S. Oei, H. Binsma, G.D. Khoe and M.K. Smit, *A fast low-power optical memory based on coupled micro-ring laser*, Nature, vol. 432, p. 206, 11 November 2004.

[13] C. Ji, M.F. Booth, A.T. Schremer and J.M. Ballantyne, *Characterizing relative intensity noise in InGaAsP-InP triangular ring lasers*, IEEE Journal of Quantum Electronics, vol. 41, no. 7, July 2005.

[14] M. Sorel, A. Scirè, G. Giuliani, R. Miglierina, S. Balle, P.J.R. Laybourn and S. Donati, *Alternate oscillations in semiconductor ring lasers*, Optics Letters, vol. 27, pp. 1992-1994, 2002.

[15] M. San Miguel and R. Toral, *Stochastic effects in physical systems, Instabilities and nonequilibrium structures VI*, E. Tirapegui, J. Martínez and R.Tiemann, Kluwer Academic Publisheres, pp. 35-130, 2000.

[16] S. Balle, P. Colet and M. San Miguel, *Statistics for the transient response of a single-mode semiconductor laser gain switching*, Physical Review A, vol.43, p. 498, 1991.

[17] K. Wiesenfeld, *Virtual Hopf phenomenon: A new precursor of period-doubling bifurcations*, Physical Review A, vol. 32, p. 1744, 1985.

[18] W.H. Press et al., *Numerical Recipes in FORTRAN 77*, Cambridge University Press, 2nd edition, 1992.

[19] C.W. Gardiner, *Handbook of stochastic methods*, Springer-Verlag, New York, 1985.

[20] R.C. Hilborn, *Chaos and nonlinear dynamics*, Oxford University Press, 2nd edition, 2000.